Published in final edited form as:
J Magn Reson Imaging. 2014 April ; 39(4): 781–788. doi:10.1002/jmri.24212.

Hybrid Multidimensional T_2 and Diffusion-Weighted MRI for Prostate Cancer Detection

Shiyang Wang, PhD[1], **Yahui Peng, PhD**[1], **Milica Medved, PhD**[1], **Ambereen N. Yousuf, MBBS**[1], **Marko K. Ivancevic, PhD**[2], **Ibrahim Karademir, MD**[1], **Yulei Jiang, PhD**[1], **Tatjana Antic, MD**[3], **Steffen Sammet, MD, PhD, DARB**[1], **Aytekin Oto, MD**[1], and **Gregory S. Karczmar, PhD**[1,*]

[1]Department of Radiology, the University of Chicago, Chicago, Illinois, USA

[2]Philips Healthcare, MRI Clinical Science, Cleveland, Ohio, USA

[3]Department of Pathology, the University of Chicago, Chicago, Illinois, USA

Abstract

Purpose—To study the dependence of apparent diffusion coefficient (ADC) and T_2 on echo time (TE) and b-value, respectively, in normal prostate and prostate cancer, using two-dimensional MRI sampling, referred to as "hybrid multidimensional imaging."

Materials and Methods—The study included 10 patients with biopsy-proven prostate cancer who underwent 3 Tesla prostate MRI. Diffusion-weighted MRI (DWI) data were acquired at b = 0, 750, and 1500 s/mm^2. For each b-value, data were acquired at TEs of 47, 75, and 100 ms. ADC and T_2 were measured as a function of b-value and TE, respectively, in 15 cancer and 10 normal regions of interest (ROIs). The Friedman test was used to test the significance of changes in ADC as a function of TE and of T_2 as a function of b-value.

Results—In normal prostate ROIs, the ADC at TE of 47 ms is significantly smaller than ADC at TE of 100 ms (P = 0.0003) and T_2 at b-value of 0 s/mm^2 is significantly longer than T_2 at b-value of 1500 s/mm^2 (P = 0.001). In cancer ROIs, average ADC and T_2 values do not change as a function of TE and b-value, respectively. However, in many cancer pixels, there are large decreases in the ADC as a function of TE and large increases in T_2 as a function of b-value. Cancers are more conspicuous in ADC maps at longer TEs.

Conclusion—Parameters derived from hybrid imaging that depend on coupled/associated values of ADC and T_2 may improve the accuracy of MRI in diagnosing prostate cancer.

Keywords

DWI; TE; T_2; ADC; multidimensional hybrid MRI; prostate cancer

*Address reprint requests to: G.K., Department of Radiology, University of Chicago Medical Center, 5841 South Maryland Avenue, Chicago, IL, 60637. gskarczm@uchicago.edu.

Drs. Karczmar and Oto share senior authorship.

PROSTATE CANCER IS the second leading cause of cancer-related mortality in men in the United States (1). MRI is currently the best noninvasive tool for imaging of prostate cancer because of its high soft tissue contrast, multiplanar capabilities, and the potential for providing unique biologic information not available with other imaging modalities. Multiparametric MR imaging, including T_2-weighted imaging, diffusion-weighted MRI (DWI), and dynamic contrast enhanced MRI (DCE-MRI), is a widely accepted tool for diagnosis, local staging, and detection of recurrence of prostate cancer (2-9).

Combinations of data from T_2-weighted imaging and DWI have been demonstrated to improve diagnostic accuracy (10,11). A recent meta-analysis concluded that combination of T_2-weighted imaging with DWI is a better tool for detection and overall evaluation of prostate cancer compared with T_2-weighted images alone, and provides a pooled sensitivity of 76% and specificity of 82% for detection of prostate cancer (12). Although this improvement is encouraging, higher sensitivity and specificity are needed for routine clinical applications of MRI.

Previous work using combinations of T_2-weighted imaging and DWI measured T_2 and apparent diffusion coefficient (ADC) independently, and thus implicitly assumed that the T_2 and ADC in each voxel are independent (10-12). However, studies of neuro-logical model systems, such as ex vivo tissues of bovine optic nerve (13) and in vivo acute cerebral infraction (14), demonstrated that T_2 and ADC are frequently coupled; that is, distinct populations of water molecules in each voxel with specific paired T_2 and ADC values can be identified. These different populations of water protons are probably heteroge-neously distributed on a microscopic level. For example, previous work (13,15) suggests that, within single voxels in brain, a population of water molecules that interacts strongly with myelin sheath along nerves has both a short T_2 and restricted, anisotropic diffusion, and that other populations of water molecules in the same voxel with different ADC and T_2 can be identified. Multiple compartments with characteristic T_2 and ADC have also been identified in muscle (16). Theoretical models of diffusion in tissue have included a compartment of intracellular water with a long T_2 and a low ADC due to restricted diffusion (17). This earlier work suggests that two-dimensional (2D) analysis can be used to analyze heterogeneous tissues, and identify populations of water molecules characterized by specific combinations of ADC and T_2. This approach may pick out specific environments that are likely to be associated with cancer, even in the presence of a large percentage of normal tissue, and therefore might increase diagnostic accuracy. This is analogous to the use of multidimensional nuclear MR spectroscopic methods to detect specific functional groups and structural features in complicated molecules with a large number of resonances (18,19). Does and Gore used this approach, which they referred to as ‘hybrid diffusion-weighted imaging’, to study compartmentation in normal and ischemic rat brain (20).

Although this approach is accurately described as 2D imaging (or multidimensional imaging if multiple independent parameters are interrogated), we refer to it as “hybrid imaging,” to distinguish it from the previous imaging studies that used both T_2 and ADC, but treated them as independent parameters. To acquire the “hybrid” data reported here, a diffusion-weighted spin echo was used to sample echo time (TE) values and “b”-values, and the resulting signal was detected with echo planar imaging (EPI) to produce a matrix of signal

inten-sities associated with each image pixel. This method was used because it is compatible with standard clinical pulse sequences available on Philips scanners.

Application of this principle to cancer has potential to produce new diagnostic parameters: the ADC in each voxel can be measured as a function of TE and the T_2 can be measured as a function of "b." The dependence of ADC on TE and of T_2 on "b" may provide novel diagnostic useful information. Thus, analysis of 2D hybrid datasets provides opportunities to develop image-based markers that may help to differentiate cancer from normal prostate and might also be sensitive to Gleason grade.

This pilot study is a first step toward evaluating the usefulness of the hybrid approach for prostate cancer diagnosis. Prostate cancers were identified on MR images based on biopsy results and contrast in T_2 and diffusion-weighted images. Hybrid data from preselected regions of interest (ROIs) in prostate cancers and normal prostatic tissue are compared. As a result, the study did not determine sensitivity and specificity of hybrid imaging for detection of prostate cancer. Rather the goals were to determine whether T_2 and ADC change as a function of "b" and "TE" and to compare the dependence of T_2 and ADC on "b" and "TE" in normal prostate and prostate cancer.

MATERIALS AND METHODS

Patients

This HIPAA-compliant prospective study was approved by our Institutional Review Board, and all participants provided written informed consent. Fifteen consecutive patients with transrectal ultrasound (TRUS)-guided biopsy proven prostate cancer that were referred to the Department of Radiology at our institution for a diagnostic MRI exam of the prostate between April 2012 and October 2012 and consented to the study were recruited. A minimum of six cores (range, 6–12) were obtained in each case (apex, mid-gland, and base from each side). Of the 15 patients consented, three patients were excluded due to no evidence of prostate cancer on MRI, and two patients were excluded because scaling information regarding the signal intensity was lost during data transfer. Fifteen cancer regions in the 10 remaining patients (average age 64.8 years, range 48–74 years; Gleason score range 6–8, median 6; serum prostate-specific antigen (PSA) median 7.06 ng/mL, range 3.53–20.34 ng/mL) were identified on MRI.

MRI Protocols

All MR examinations were performed using a 3.0 Tesla (T) scanner (AchievaTX, Philips Healthcare). An endorectal coil combined with a six-channel phasedarray cardiac coil was used for all examinations. Immediately before the MR examination, 1 mg of glucagon was injected intramuscularly to reduce intestinal motility. For anatomic reference, the entire prostate was imaged in the axial plane, with slices positioned to be perpendicular to the rectal wall, guided by sagittal images. The following images were obtained: axial, coronal, and sagittal T_2 weighted turbo spin-echo (TSE) (slice thickness, 3 mm; echo time/repetition time TE/TR = 115/4589 ms, 1 echo, TSE factor = 17, number of averages = 2), axial T_1-

weighted TSE (TE/ TR = 8.0/556 ms), axial T_2 maps (TR = 2000–2337 ms, TE = 0–100 ms, with 20 ms increments), and axial DCE-MRI.

For hybrid DWI/T_2 measurements, diffusion-weighted images were acquired in the axial plane with free breathing. The DWI pulse sequence was a standard pelvic prostate DWI protocol (Philips Medical Systems, Netherlands) composed of a single spin echo module with diffusion sensitizing gradients placed symmetrically around the 180 degree pulse, followed by a single-shot EPI module for signal detection (180 x 180 mm^2 field of view with 2.5 x 2.5 mm^2 in plane resolution, 128 x 128 reconstruction matrix giving a 1.4 × 1.4 × 3 mm^3 voxel size). Data were acquired with b-values of 0, 750, and 1500 s/mm^2 and TEs of 47 ms, 75 ms, and 100 ms. TR was 3000 ms, spectrally adiabatic inversion recovery (SPAIR) module was used for fat saturation; NEX = 4, total scan time was 7.0–8.7 min. In this case, “TE” refers to the length of the spin echo diffusion-sensitizing module. This provides a 2D, 3 x 3 array of measurements for each image pixel; each measurement is associated with different “b” and “TE” values. Because a standard Philips DWI sequence was used, increased TE at constant “b”-value resulted in increased separation between the two diffusion gradients (Δ), and reduced gradient amplitude; “Δ” increased from 24.5 ms to 77.5 ms when TE was increased from 47 ms to 100 ms. The “δ” was 11.8 ms and was constant for all three TEs.

A water phantom was used to test the performance of the pulse sequence. The measured mean ADC (2.20×10^{-3} mm^2/s) was consistent with the standard value for pure water at 20° C. In addition, studies of phantoms did not show any change in T_2 as a function of b-value or any change in ADC as a function of TE.

Data Analysis

A radiologist with 10 years of experience in prostate MRI (AO) reviewed MR images together with TRUS guided biopsy results. The tumor regions were identified as focal low signal intensity lesions on T_2-weighted images, high signal intensity on diffusion-weighted images, and homogenously dark foci on ADC maps in sextants that were biopsy positive. Normal regions were identified in the peripheral zone as homogenously hyperintense areas on T_2-weighted images, low signal on diffusion-weighted images, and high signal areas on ADC maps in sextants with no tumor based on biopsy results. ROIs were drawn on T_2-weighted images or ADC maps and were transferred to images acquired using the other pulse sequences. The Gleason score for each tumor region was also recorded based on sextant specific TRUS guided biopsy results. Voxel-wise T_2 values for each b-value were calculated from signals acquired at the three TEs using a least-squares fit to the formula:

$$S(t) = A \quad exp\left(-\frac{TE}{T2(b)}\right). \quad (1)$$

R_2 values ($1/T_2$) were also calculated and used in 2D plots, to better represent the voxels with very long T_2 values. Voxel-wise ADCs were calculated for each “TE” from signal acquired at the three b-values, using a least-squares fit to the formula:

$$S(t) = A \quad exp(-b \times ADC(TE)). \quad (2)$$

The contrast-to-noise ratios for cancers relative to normal tissue were estimated in ADC and T_2 maps as a function of "TE" and "b," respectively. The contrastto-noise ratio (CNR) was calculated as:

$$CNR = (S_C - S_{NT})/\sigma, \quad (3)$$

where SC is the average signal in the cancer ROI, SNT is the average signal in the adjacent tissue region including all voxels that are two voxels or less from the cancer ROI edges, and s is the standard deviation of signal in the normal ROI outlined for the same patient.

Statistical Analysis

The Mann-Whitney U test was used to test for statistical significance in the ADC or T_2 value differences between prostate cancer foci and normal prostate ROIs. The Friedman test was used to test for statistical significance in the differences among ADC values measured at different TEs, among T_2 values measured at different b-values, and among cancer ROI contrast-to-noise ratios at different TEs and different b-values. The average ADC, T_2, and contrast-to-noise ratio value within an ROI were used in these statistical tests. All statistical tests were two-sided. A P value less than 0.05 was considered to be statistically significant; after a Bonferroni correction for 12 multiple comparisons, $P < 0.0042$ was considered statistically significant.

RESULTS

Variation of ADC as a Function of TE

The average ADC values estimated from scans at different TE values all show a significant difference between prostate cancer ROIs and normal prostatic tissue ROIs (Table 1). For example, at TE=47 ms, the ADC averaged over all normal prostatic pixels in the selected ROIs is 1.40±6 0.24 × 10^{-3} mm^2/s versus 0.89±6 0.23 × 10^{-3} mm^2/s averaged over all pixels in the selected cancer ROIs, and this difference is statistically significant ($P < 0.001$). In prostate cancers, the average ADC values do not change significantly as a function of TE; the average ADC is 0.89±6 0.22 × 10^{-3} mm^2/s at TE = 47 ms and 0.95±6 0.32 × 10^{-3} mm^2/s at TE = 100 ms. In contrast, the average ADC in normal prostatic tissue ROIs increases significantly at longer TEs; $ADC_{TE=47}$ =1.40±6 0.18 × 10^{-} mm^2/s and $ADC_{TE=100}$=1.66±0.19 × 10^{-3} mm^2/s (P=0.0003). The dependence of the calculated ADC on TE is illustrated by the plots of the $ADC_{TE=47}$ versus $ADC_{TE=100}$ for each voxel in all ROIs (Fig. 1A) Figure 1B shows the change in ADC as a function of TE on a pixel-by-pixel basis (ΔADC; $ADC_{TE=47}$-$ADC_{TE=100}$). The average ΔADC is much closer to zero for cancer pixels (–0.026 × 10^{-3} mm^2/s) than for normal tissue (−0.265 × 10^{-3} mm^2/s), and this difference is statistically significant (P <0.001). Figure 1 demonstrates that for almost all pixels in normal prostate $ADC_{TE=100}$ is greater than $ADC_{TE=47}$, while in many cancer pixels $ADC_{TE=100}$ is less than $ADC_{TE=47}$. An alternative interpretation of Figure 1 is that the

difference between $ADC_{TE=100}$ and $ADC_{TE=47}$ decreases, and eventually becomes negative as $ADC_{TE=47}$ decreases.

Although $ADC_{TE=100}$ and $ADC_{TE=47}$ are significantly correlated, the range of different $ADC_{TE=100}$ values that correspond to each $ADC_{TE=47}$ is large (typically greater than twofold). The relationship between $ADC_{TE=100}$ and $ADC_{TE=47}$ is significantly different in cancers versus normal prostate. In cancer ROIs, the slope of the linear regression of $ADC_{TE=100}$ versus $ADC_{TE=47}$ is 0.87, while in normal tissue ROIs the slope is 1.17 ($P < 0.001$). In regions of the plot in Figure 1B where there is significant overlap between $ADC_{TE=47}$ for cancer and normal tissue (between $ADC_{TE=47}=0.9 \times 10^{-3}$ mm^2/s and 1.3×10^{-3} mm^2/s), the average ΔADC ($ADC_{TE=47}$-$ADC_{TE=100}$) is less negative for cancer pixels ($-0.0760.17 \pm 10^{-3}$ mm^2/s) than for normal tissue ($-0.2860.13 \pm 10^{-3}$ mm^2/s), and this difference is highly statistically significant when the pixels in the overlap region are treated as independent data points.

Variation of T_2 and R_2 as a Function of b-Values

The average T_2 values in selected ROIs in normal prostatic tissue and cancer are significantly different: 330 ± 208 ms in normal prostate versus 106 ± 52 ms in cancer at b = 0 s/mm^2 (P = 0.003; Table 2). The average T_2 values of cancer ROIs decrease slightly, but not significantly, from 106 6 52 ms to 95 6 70 ms ($P = 0.42$), as b-value increases from 0 to 1500 s/ mm^2. In contrast, T_2 in normal prostate decreases significantly ($P = 0.001$) with increasing "b." $T_{2:b=0}$ is on average 330 ± 208 ms and $T_{2:b=1500}$ is on average 113 ± 77 ms. The results are illustrated by plots of the $R_{2:b=0}$ ($1/T_2$) versus $R_{2:b=1500}$, and DR_2 versus $R_{2:b=0}$ in Figure 2. Figure 2A demonstrates that for almost all pixels in normal prostate $R_{2:b=0}$ is less than $R_{2:b=1500}$, whereas this is not true for cancer pixels. In Figure 2B, the average ΔR_2 ($R_{2:b=0}-R_{2:b=1500}$) is different for cancers (-0.0008 ms^{-1}) than for normal tissue (-0.007 ms^{-1}), and this difference is statistically significant ($P<0.001$). While ΔR_2 ($R_{2:b=0}-R_{2:b=1500}$) is almost always less than zero in pixels from normal prostate, ΔR_2 is positive for over half of the pixels from cancers.

In both normal and cancer pixels, $R_{2:b=0}$ and $R_{2:b=1500}$ are moderately correlated (correlation coefficients are r=0.46 and r=0.36, respectively), and the correlation coefficient between $R_{2:b=0}$ and Δ(R**2**) are r=0.41 and r=0.64 ($P<0.0001$; see Fig. 2B). However, the relationship between $R_{2:b=0}$ and $R_{2:b=1500}$ is significantly different in cancers versus normal prostate. In cancers, the slope of linear regression of $R_{2:b=0}$ versus $R_{2:b=1500}$ is 0.32, while in normal tissue, the slope is 0.53 (p<0.0001). In regions of the plot in Figure 2B where there is significant overlap between $R_{2:b=0}$ for cancer and normal tissue (between $R_{2:b=0}$=0.0075 ms^{-1} and 0.015 ms^{-}1), the average ΔR_2 ($R_{2:b=0}-R_{2:b=1500}$) is different for cancers (-0.001 ± 004 ms^{-}1) than for normal tissue (-0.0066 ± 003 ms^{-1}), and this difference is highly statistically significant when the pixels in the overlap region are treated as independent data points.

Figure 3A shows images of ADC at TE=47, 75, and 100 ms, and the subtracted images, "$ADC_{TE=47}-$ $ADC_{TE=100}$." The increased contrast showing the tumor more clearly is evident in the $ADC_{TE=100}$ image and the subtracted image. Figure 3B shows T_2 images for the same cancer as in Figure 3A, at b=0, 750, and 1500 s/mm^2. The contrast for cancer

versus normal tissue is higher at low b-value, and in the subtracted image ($T_{2:b=0}$-$T_{2:b=1500}$). Figures 3C and 3D show box plots of average contrast-to-noise ratio (from Eq. (3)) for the tumor ROIs compared with the surrounding tissue on ADC and T_2 maps, as a function of "TE" and "b," respectively. The contrast-to-noise ratio in ADC maps is significantly higher (P=0.02) at TE=100 ms compared with TE=47 ms. Contrast-to-noise ratio in T_2 maps is significantly higher (*P*=0.001) with b=0 s/mm^2 compared with b=1500 s/mm^2.

DISCUSSION

In pixels with high $T_{2:b=0}$, primarily pixels in normal prostate, T_2 decreases markedly at high b-values. In pixels with lower $T_{2:b=0}$, primarily tumor pixels, the average T_2 decreases slightly with increasing b-value. However, in many pixels with low $T_{2:b=0}$, particularly pixels identified as cancer, there are large increases in T_2 with increasing b-value. In pixels with higher $ADC_{TE=47}$, primarily pixels in normal prostate, ADC increases as a function of TE. In contrast, in pixels with lower $ADC_{TE=47}$, primarily cancer pixels, there is relatively little change in average ADC as a function of TE. However, in a large percentage of pixels with lower $ADC_{TE=47}$, predominantly pixels from cancers, there is a decrease in ADC as a function of TE. Thus, the coupling or association between ADC and T_2 appears to be markedly different in cancers compared with normal prostate.

The results suggest modest correlation between ADCs measured at different TEs, and between T_2 values measured at different b-values. If the ADC at TE = 47 ms could be reliably predicted from the ADC at TE = 100 ms, and if T_2 at b=0 s/mm^2 could be reliably predicted from T_2 at b=1500 s/mm^2, then hybrid, 2D imaging would not provide new information. However, differences in the plots for cancer pixels versus normal pixels in Figures 1 and Figure 2 suggest that this is not the case. The slopes of the linear regression lines through data from cancer pixels and normal pixels, for plots of $ADC_{TE=47}$ versus $ADC_{TE=100}$ and plots of $R_{2:b=0}$ versus $R_{2:b=1500}$, are significantly different. In addition, in areas where $ADC_{TE=47}$ and $R_{2:b=0}$ values for cancer and normal pixels overlap, changes in ADC as a function of TE and R_2 as a function of b-value differentiate cancer from normal prostate. These results suggest that the coupling/association between T_2 and ADC can differentiate between cancer and normal tissue. However, it should be emphasized that these results apply to the pooled data from all patients and all ROIs. It is not possible to evaluate the diagnostic value of these relationships, based on the small number of cases reported here.

The scatter around the best-fit lines through the plots in Figures 1A and 2A is large compared with the expected random variation in ADC and R_2 measurements. For example, the coefficient of variation for in vivo ADCs is reported to be approximately 14% in ROIs in the liver, spleen, and pancreas (21). Although coefficients of variation due to random error for single pixels are expected to be larger, the observed variations of twofold and greater in the $ADC_{TE=47}$ values associated with each $ADC_{TE=100}$ value, and the even larger variations in the values of $R_{2:b=0}$ associated with each value of $R_{2:b=1500}$ (see Figures 1 and 2) may reflect local biology and physiology. This suggests that hybrid imaging is sensitive to local properties that may differentiate cancer from normal prostatic tissue, and cannot be detected by conventional methods.

These results are consistent with a simple model of prostatic tissue. Normal prostate tissue has a large number of glands with large lumina. Fluid in the glandular lumina is likely to have a long T_2 and a high ADC (22). The hybrid approach selects for water protons that combine both of these characteristics. Strong diffusion sensitizing gradients attenuate signal from rapidly diffusing spins in the glandular lumen, and thus emphasize shorter T_2 signals from other regions of normal prostate. Alternatively, long echo times emphasize long T_2 signals in prostatic glands, and these signals are characterized by a high ADC. Thus, our data are consistent with the presence of at least two populations of water protons in the normal tissue, one with long T_2 and high ADC, and one with comparatively shorter T_2 and lower ADC. A large decrease in ADC at long TE, and a large decrease in T_2 at high b-value, may be more reliable markers for high luminal volume fraction than either ADC or T_2 measured independently.

Glandular luminal volume is lower in cancers than in normal tissue, with the percentage of luminal volume decreasing on average as Gleason grade increases (23). As a result, the average T_2 in cancers is generally shorter than in normal prostatic tissue. However, these preliminary results suggest that “hybrid” measurements at high b-values detect a population of water molecules with a relatively long T_2 within some pixels in cancer ROIs. This may represent extracellular water with restricted diffusion through densely packed cancer cells and a relatively long T_2 (16,24). Alternatively, this may represent intracellular water with restricted diffusion, consistent with previous publications suggesting that intracellular water in cancers has a relatively long T_2 compared with intracellular water in normal tissue (25). In either case, a signal with long T_2 coupled to, or associated with low ADC may be characteristic of cancers, and isolation of this signal using a hybrid approach may increase diagnostic accuracy. Hybrid imaging might be particularly useful when cancers are diffuse and intermixed with a large percentage of normal prostatic tissue. In such cases, hybrid imaging could filter out the bulk signal from normal tissue, and identify a relatively small population of cancer cells, based on specific combinations of coupled or associated parameters, including T_2 and ADC.

The characteristics of different tissue compart-ments (e.g. intracellular, extracellular, lumen, etc.) can be inferred from analysis of the dependence of ADC and T_2 on TE and b-value, as discussed here. Alternatively, compartments could be evaluated more explicitly by fitting hybrid data to two or more exponential terms, each a function of a different combination of ADC and T_2 values, and each with an amplitude indicating the size of each compartment. This approach might increase diagnostic accuracy, by reliably identifying specific compartments with characteristics (e.g., ADC and T_2 values) associated with cancer. Scans of more patients, with histopathologic correlation will be required to develop appropriate models for hybrid data from normal prostatic tissue and cancers.

The results show that contrast between cancers and normal tissue, and morphologic detail can be improved with hybrid imaging. Cancers were detected with higher contrast in ADC maps acquired at longer TEs, and more complete sampling of the 2D parameter space may identify parameters that produce ADC maps with maximum conspicuity of cancers. Alternatively, data from 2D hybrid imaging could be used to synthesize ADC maps with an optimal contribution from T_2 to maximize tumor conspicuity. In T_2 maps, cancers were

most conspicuous with the nominal b-value set to zero. However, the true b-value for these images was not zero because of the rapidly switching gradients used in the echo-planar imaging sequence. Cancers might be detected with even higher contrast if pulse sequences with minimal sensitivity to diffusion are used for signal acquisition. Alternatively, hybrid data could be used to estimate a pure T_2 image with minimal diffusion-weighting.

This study has several limitations:

These preliminary results suggest that cancers and normal tissue can be separated based on differences in the functional dependence of ADC on TE and of T_2 on b-value. However, there are other plausible explanations for these results. For example, the results could simply reflect differences between water protons with low and high ADC, or low and high T_2. The relationship between ADC and TE, and between T_2 and b-value may be nonlinear; this could explain the apparent differences in the plots for cancer and normal pixels shown in Figures 1 and 2. More studies with phantoms and detailed correlation of hybrid data with histopathology will be necessary to definitively test the diagnostic utility of hybrid data.

Hybrid analysis was performed on cancer and normal ROIs chosen by an experienced radiologist according to the biopsy results, T_2-weighted images, and diffusion-weighted images. Therefore, the study was not designed to evaluate the diagnostic accuracy of hybrid imaging. Instead, the goal was to determine the interdependence of the ADC and T_2 and characterize hybrid data from normal prostate and cancer. A larger clinical trial will be required to evaluate diagnostic accuracy.

The study included data from a relatively small number of patients (n = 10) with a small range of Gleason scores and cancer stages and, therefore, was not powered to precisely define the characteristics of cancers and normal tissue, or to evaluate the sensitivity of hybrid parameters to Gleason score. Because the subjects did not receive a prostatectomy, detailed correlation of hybrid data with histopathology was not possible. A more rigorous evaluation of the hybrid approach will require a study of patients who subse-quently receive a prostatectomy.

In this study, a commercially available Philips DWI pulse sequence was used to acquire hybrid data. For a constant “b” value, this sequence increases separation between diffusion sensitizing gradients, “Δ,” and reduces the amplitudes of diffusion-sensitizing gradients as “TE” increases. This may affect sensitivity to restricted diffusion (26). The SPAIR fat suppression module may also affect the results.

The number and range of “TE” values sampled, and the number of b-values sampled was modest. The shortest TE was limited by the slew rate, gradient duration (δ) and the value of Δ required to achieve large b-values. The number of values of “b” and “TE” sampled was limited by the need to limit total exam times in these pilot studies. In the future, improvements in pulse sequence design and dedicated research exams that allow more time for hybrid data acquisition will address these problems.

Estimates of contrast-to-noise ratio were based on the assumption that the signal from normal prostatic tissue surrounding lesions should be homogeneous, and that signal

variation in these regions is primarily due to noise. More accurate estimates of contrast-to-noise ratio and signal-to-noise ratio will require repeated hybrid acquisitions.

In conclusion, these preliminary results suggest potential advantages of 2D hybrid acquisition and analysis of DWI and T_2 data for prostate cancer diagnosis. While conventional "multidimensional" MRI implicitly considers T_2 and ADC to be independent, the hybrid method considers T_2 and ADC as coupled or associated parameters. The ADC is evaluated as a function of "TE", and the T_2 is evaluated as a function of b-value in each voxel. This approach may produce new image-based markers for prostate cancer. In addition, hybrid imaging provides new methods for increasing lesion conspicuity in MR images and improving depiction of morphology, e.g., by producing ADC maps at long TEs, or by calculating T_2 maps with minimal sensitivity to diffusion. Although 2D diffusion- and T_2-dependent hybrid imaging is discussed here, in principle this approach can be extended to include a larger number of dimensions and contrast mechanisms (e.g., T_1, T_2*, magnetization transfer, spin tagging, etc.). The hybrid method presented here, as well as generalizations of this approach, may pick out subpopulations of water protons in the micro-environment that are associated with cancers and thus increase diagnostic accuracy.

Acknowledgments

Philips Medical Systems

Novel approaches to DWI

University of Chicago Cancer Center

5 P50CA014599.

REFERENCES

1. ACS. Cancer facts and figures. 2012. Available from: http://www.cancer.org/acs/groups/content/@epidemiologysurveilance/ documents/document/acspc-031941.pdf
2. ESUR. 2012. Available from: http://www.esur.org/Contrast-media.51.0.html
3. Fuchsjäger M, Akin O, Shukla-Dave A, Pucar D, Hricak H. The role of MRI and MRSI in diagnosis, treatment selection, and post-treatment follow-up for prostate cancer. Clin Adv Hematol Oncol. 2009; 7:193–202. [PubMed: 19398944]
4. Mazaheri Y, Shukla-Dave A, Muellner A, Hricak H. MRI of the prostate: clinical relevance and emerging applications. J Magn Reson Imaging. 2011; 33:258–274. [PubMed: 21274967]
5. Turkbey B, Choyke PL. Multiparametric MRI and prostate cancer diagnosis and risk stratification. Curr Opin Urol. 2012; 22:310–315. [PubMed: 22617060]
6. Bittencourt LK, Barentsz JO, de Miranda LC, Gasparetto EL. Prostate MRI: diffusion-weighted imaging at 1.5T correlates better with prostatectomy Gleason Grades than TRUS-guided biopsies in peripheral zone tumours. Eur Radiol. 2012; 22:468–475. [PubMed: 21913058]
7. Yakar D, Debats OA, Bomers JG, et al. Predictive value of MRI in the localization, staging, volume estimation, assessment of aggressiveness, and guidance of radiotherapy and biopsies in prostate cancer. J Magn Reson Imaging. 2012; 35:20–31. [PubMed: 22174000]
8. Akin O, Gultekin DH, Vargas HA, et al. Incremental value of diffusion weighted and dynamic contrast enhanced MRI in the detection of locally recurrent prostate cancer after radiation treatment: preliminary results. Eur Radiol. 2011; 21:1970–1978. [PubMed: 21533634]
9. Vargas HA, Akin O, Franiel T, et al. Diffusion-weighted endorectal MR imaging at 3 T for prostate cancer: tumor detection and assessment of aggressiveness. Radiology. 2011; 259:775–784. [PubMed: 21436085]

10. Gibbs P, Liney GP, Pickles MD, Zelhof B, Rodrigues G, Turnbull LW. Correlation of ADC and T2 measurements with cell density in prostate cancer at 3.0 Tesla. Invest Radiol. 2009; 44:572–576. [PubMed: 19692841]
11. Soylu FN, Peng Y, Jiang Y, et al. Seminal vesicle invasion in prostate cancer: evaluation by using multiparametric endorectal MR imaging. Radiology. 2013; 267:797–806. [PubMed: 23440325]
12. Wu LM, Xu JR, Ye YQ, Lu Q, Hu JN. The clinical value of diffu-sion-weighted imaging in combination with T2-weighted imaging in diagnosing prostate carcinoma: a systematic review and meta-analysis. AJR Am J Roentgenol. 2012; 199:103–110. [PubMed: 22733900]
13. Stanisz GJ, Henkelman RM. Diffusional anisotropy of T2 compo-nents in bovine optic nerve. Magn Reson Med. 1998; 40:405–410. [PubMed: 9727943]
14. Burdette JH, Elster AD, Ricci PE. Acute cerebral infarction: quantification of spin-density and T2 shine-through phenomena on diffusion-weighted MR images. Radiology. 1999; 212:333–339. [PubMed: 10429687]
15. Madler B, Drabycz SA, Kolind SH, Whittall KP, MacKay AL. Is diffusion anisotropy an accurate monitor of myelination? Correlation of multicomponent T2 relaxation and diffusion tensor anisotropy in human brain. Magn Reson Imaging. 2008; 26:874–888. [PubMed: 18524521]
16. Ababneh Z, Beloeil H, Berde CB, Gambarota G, Maier SE, Mulkern RV. Biexponential parameterization of diffusion and T2 relaxation decay curves in a rat muscle edema model: decay curve components and water compartments. Magn Reson Med. 2005; 54:524–531. [PubMed: 16086363]
17. Zhong JH, Gore JC. Studies of restricted diffusion in heterogeneous media containing variations in susceptibility. Magn Reson Med. 1991; 19:276–284. [PubMed: 1881316]
18. Kumar A, Wagner G, Ernst RR, Wüthrich K. Studies of J-connectives and selective 1H-1H Overhauser effects in H2O solutions of biological macromolecules by two-dimensional NMR experiments. Biochem Biophys Res Commun. 1980; 96:1156–1163. [PubMed: 6159893]
19. Nagayama K, Wuthrich K, Ernst RR. Two-dimensional spin echo correlated spectroscopy (SECSY) for 1H NMR studies of biological macromolecules. Biochem Biophys Res Commun. 1979; 90:305–311. [PubMed: 496980]
20. Does MD, Gore JC. Compartmental study of diffusion and relaxation measured in vivo in normal and ischemic rat brain and trigeminal nerve. Magn Reson Med. 2000; 43:837–844. [PubMed: 10861878]
21. Braithwaite AC, Dale BM, Boll DT, Merkle EM. Short- and mid-term reproducibility of apparent diffusion coefficient measurements at 3.0-T diffusion-weighted imaging of the abdomen. Radiology. 2009; 250:459–465. [PubMed: 19095786]
22. Fan X, Haney CR, Agrawal G, et al. High-resolution MRI of excised human prostate specimens acquired with 9.4T in detection and identification of cancers: validation of a technique. J Magn Reson Imaging. 2011; 34:956–961. [PubMed: 21928309]
23. Tabesh A, Teverovskiy M, Pang HY, et al. Multifeature prostate cancer diagnosis and Gleason grading of histological images. IEEE Trans Med Imaging. 2007; 26:1366–1378. [PubMed: 17948727]
24. Saab G, Thompson RT, Marsh GD, Picot PA, Moran GR. Two-dimensional time correlation relaxometry of skeletal muscle in vivo at 3 Tesla. Magn Reson Med. 2001; 46:1093–1098. [PubMed: 11746574]
25. Ling GN, Tucker M. Nuclear magnetic resonance relaxation and water contents in normal mouse and rat tissues and in cancer cells. J Natl Cancer Inst. 1980; 64:1199–1207. [PubMed: 6929018]
26. Kim S, Chi-Fishman G, Barnett AS, Pierpaoli C. Dependence on diffusion time of apparent diffusion tensor of ex vivo calf tongue and heart. Magn Reson Med. 2005; 54:1387–1396. [PubMed: 16265644]

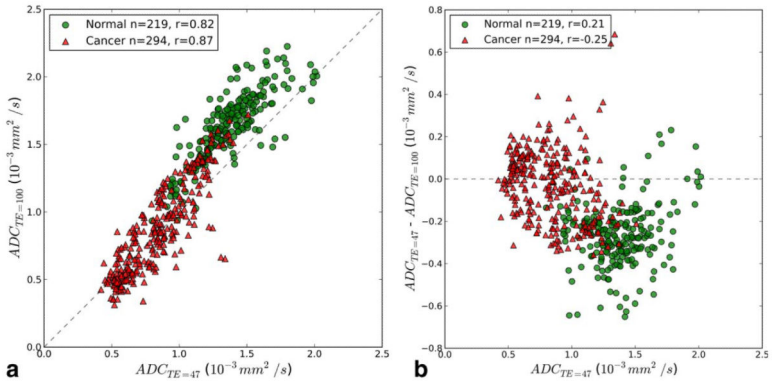

Figure 1.

A: A scatter plot of voxel-wise ADC values at two TEs. The dashed line is the identity line. Red triangles are cancer pixels, green circles are normal pixels. The number of voxels (n) and the Pearson correlation coefficient (r) are reported in the legend. B: A scatter plot of voxel-wise $ADC_{TE=47}$ versus $ADC_{TE=47}$-$ADC_{TE=100}$. Red triangles are cancer pixels; green circles are normal pixels. The dashed line is the zero-difference line. The number of voxels (n) and the Pearson correlation coefficient (r) are reported in the legend

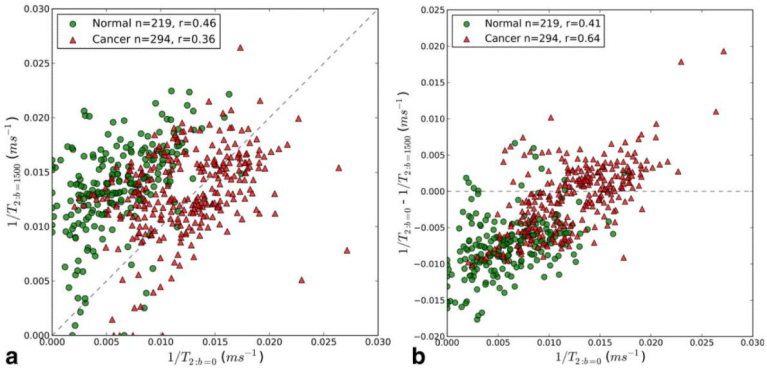

Figure 2.

A: A scatter plot of voxel-wise $1/T_2$ values estimated from scans at two different b-values. Red triangles are cancer pixels, green circles are normal pixels. The dashed line is the identity line. The number of voxels (n) and the Pearson correlation coefficient (r) are reported in the legend. **B:** A scatter plot of voxel-wise $1/T_{2:b=0}$ versus $1/T_{2:b=0} - 1/T_{2:b=1500}$. Red triangles are cancer pixels, green circles are normal pixels. The dashed line is the zero difference line. The number of voxels (n) and the Pearson correlation coefficient (r) are reported in the legend.

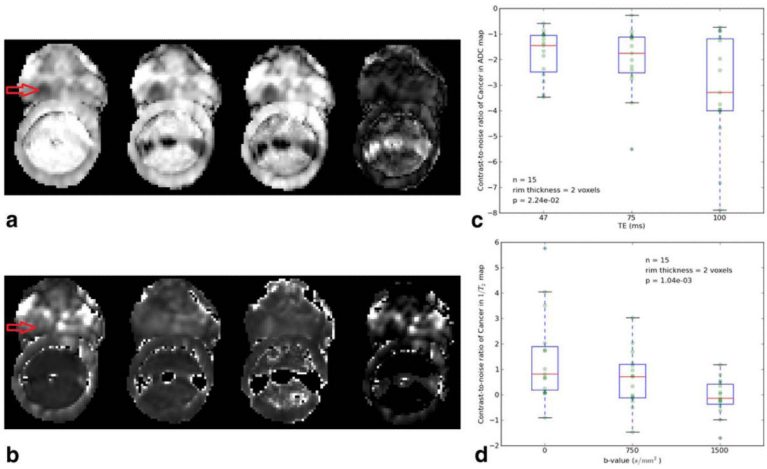

Figure 3.

A: Axial ADC images from a 71-year-old patient with prostate cancer are shown. Images from left to right are: ADC at TE = 47, 75, 100 ms and the absolute value of the difference image: $ADC_{TE=47}$-$ADC_{TE=100}$ (arrow points to cancer location: right mid medial, Gleason score 8). Scale is the same for the first three images, and the last image was scaled from 0 to the maximum signal in the difference image. The increased contrast showing the tumor more clearly is evident in $ADC_{TE=100}$ and the subtraction image. **B:** Same patient and slice as in Figure 3a is shown. Conventional images of T_2 at b=0, 750, 1500 s/mm^2 and the absolute value of the subtraction image, $T_{2:b=0}-T_{2:b=1500}$, are shown. All the images are set to the same scale. Increased contrast appears in the cancer region (right mid medial, Gleason score 8) compared with normal region (right mid lateral) at b=0 and in the subtraction image. The images were scaled identically. **C:** Boxplot of estimated contrast-to-noise ratio for ADC values in the 15 prostate cancer ROIs, at different TEs. **D:** Boxplot of contrast-to-noise ratios for $1/T_2$ values in the 15 prostate cancer ROIs, at different b-values.

Table 1

Average ADC Values ($\times 10^{-3}$ mm^2/s) Calculated From Scans With Different TEs, for Prostate Cancer and Normal Tissue ROIs

Echo time (ms)	Cancer (n=15)	Normal (n=10)	*P* value*
47	0.89 ± 0.22	1.40 ± 0.18	0.00009
75	0.93 ± 0.26	1.55 ± 0.20	0.00009
100	0.95 ± 0.32	1.66 ± 0.19	0.00006
P value†	0.94	0.0003	

*Mann-Whitney test comparing cancer and normal ROIs.

†Friedman rank sum test comparing ADC values at 47, 75, and 100 ms.

Table 2

Average T_2 Values (ms) Estimated From Scans With Different b-Values, in Prostate Cancer and Normal Tissue ROIs

b value (s/mm^2)	Cancer (n=15)	Normal (n=10)	*P* value*
0	106 ± 52	330 ± 208	0.003
750	85 ± 21	140 ± 81	0.06
1500	95 ± 70	113 ± 77	0.64
P value†	0.42	0.001	

*Mann-Whitney test comparing cancer and normal ROIs.

†Friedman rank sum test comparing T_2 values at b=0, 750, and 1500 s/mm^2.